aerospace

MDPI

Article

Lessons Learned in Designing a Proposed Ultraviolet Sterilization System for Space

David W. Hughes [1], Giuseppe Cataldo [1,*], Fernando A. Pellerano [1], Terra C. Hardwick [1], Frankie Micalizzi [1], Victor J. Chambers [1], Brian R. Bean [2], Berton J. Braley [3], William B. Cook [1], Ratna Day [4], Thomas J. Emmett [1], Clark D. Hovis [1], Stefan Ioana [5], Dillon E. Johnstone [6], Amandeep Kaur [1], Wendy M. Morgenstern [1], Nicholas M. Nicolaeff [5], Lawrence Ong [7], Len Seals [1], Richard G. Schnurr [1], Laurie L. Seide [7], George B. Shaw [1], Kevin A. Smith [8], Oscar Ta [9], William J. Thomes [1] and Honam Yum [7]

[1] NASA Goddard Space Flight Center, Greenbelt, MD 20771, USA; david.w.hughes@nasa.gov (D.W.H.); terra.hardwick@nasa.gov (T.C.H.); frankie.micalizzi@nasa.gov (F.M.); victor.j.chambers@nasa.gov (V.J.C.); william.b.cook@nasa.gov (W.B.C.); thomas.emmett@nasa.gov (T.J.E.); clark.d.hovis@nasa.gov (C.D.H.); amandeep.kaur-1@nasa.gov (A.K.); wendy.m.morgenstern@nasa.gov (W.M.M.); len.seals@nasa.gov (L.S.); richard.g.schnurr@nasa.gov (R.G.S.); george.b.shaw@nasa.gov (G.B.S.); william.j.thomes@nasa.gov (W.J.T.)
[2] Intuitive Machines, Houston, TX 77059, USA; brian.r.bean@nasa.gov
[3] Lentech, Inc., Hanover, MD 21076, USA; berton.j.braley@nasa.gov
[4] ASRC Federal, Beltsville, MD 20705, USA; ratna.day@nasa.gov
[5] Aerodyne Industries, LLC, Cape Canaveral, FL 32920, USA; stefanioana2007@gmail.com (S.I.); nicholas.m.nicolaeff@nasa.gov (N.M.N.)
[6] Science Systems and Applications, Inc., Lanham, MD 20706, USA; dillon.e.johnstone@nasa.gov
[7] KBR, Inc., Fulton, MD 20759, USA; lawrence.ong@nasa.gov (L.O.); laura.l.seide@nasa.gov (L.L.S.); honam.yum@nasa.gov (H.Y.)
[8] Design Interface, Inc., Finksburg, MD 21048, USA; kevin.a.smith@nasa.gov
[9] Genesis Engineering Solutions, Inc., Lanham, MD 20706, USA; oscar.ta@nasa.gov
* Correspondence: giuseppe.cataldo@nasa.gov

Abstract: This paper presents a number of lessons learned while designing a proposed sterilization system for Mars Sample Return. This sterilization system is needed to inactivate any potentially hazardous Mars material on the exterior surface of the vessel containing sealed sample tubes filled with Mars rock cores, regolith and atmosphere. These returned samples would provide information on the geologic history of Mars, the evolution of its climate and the potential for ancient life. Mars Sample Return is categorized at Planetary Protection Category V Restricted Earth Return, so it is required to protect the Earth–Moon system from the biological impact of returning samples from Mars to Earth. This article reviews lessons learned in the development of a particular engineering implementation to support the protection of the Earth–Moon biosphere: the use of in situ ultraviolet LED illumination. The details of the biological efficacy of this approach or the policy-related impacts are outside of the scope of this manuscript. The lessons learned presented here include establishing design requirements for the system, the selection of a light source, optical design options, contamination control and approaches to thermal and power management.

Keywords: planetary protection; UV; LED; sterilization

Citation: Hughes, D.W.; Cataldo, G.; Pellerano, F.A.; Hardwick, T.C.; Micalizzi, F.; Chambers, V.J.; Bean, B.R.; Braley, B.J.; Cook, W.B.; Day, R.; et al. Lessons Learned in Designing a Proposed Ultraviolet Sterilization System for Space. *Aerospace* **2024**, *11*, 538. https://doi.org/10.3390/aerospace11070538

Academic Editor: Ralf Srama

Received: 29 March 2024
Revised: 19 June 2024
Accepted: 26 June 2024
Published: 1 July 2024

1. Introduction

The Mars Sample Return (MSR) Program is a joint NASA–European Space Agency (ESA) effort aimed at bringing to Earth samples of Martian rock cores, regolith and atmosphere. The goal is to answer key questions about the geologic and climate history of Mars, including the potential for ancient life [1–5]. The management of the returned Martian samples to prevent the contamination of Earth's biosphere from potentially hazardous biological Martian material is a requirement mandated by NASA [6] and ESA [7]. This requirement is guided by the policies of the Committee on Outer Space Research (COSPAR) [8] and addresses Article IX of the United Nations' Outer Space Treaty of 1967 [9].

The approach selected by the MSR Program involves the use of redundant containment for any non-sterilized Mars material and the sterilization of any potentially harmful Mars biology that might proliferate and compromise the integrity of Earth's biosphere [6,10].

This paper describes the challenges and lessons learned while designing a system to deliver ultraviolet (UV) light with the intent to sterilize the exterior of the sample containment vessel, known here as the Orbiting Sample (OS). The OS would contain up to 30 sealed sample tubes of Martian rock cores, regolith and atmosphere, which are being collected by the Perseverance rover [11–14].

This paper is based on the MSR architecture described in Ref. [15], where the OS would be delivered from Mars orbit to the NASA-provided Capture, Containment and Return System (CCRS), which sits on top of the ESA-provided Earth Return Orbiter (ERO) [10,16]. The ERO would detect the OS in Mars orbit and enable the CCRS to capture it inside a capture cone. The CCRS would then funnel the OS into a mechanism that orients and positions the OS for robotic installation into the Earth Entry System (EES) (Figure 1). However, before that installation may take place, the surface of the OS must be sterilized to inactivate any potentially hazardous Mars material on the exterior surface of the OS, so that it can function as the first of two containment vessels. The CCRS UV system (UVS) is positioned to deliver light to the OS robotic pickup interface while it is still held in the Orientation Mechanism and then to irradiate the remaining surfaces as the robotic arm draws the OS through the UVS (Figure 2).

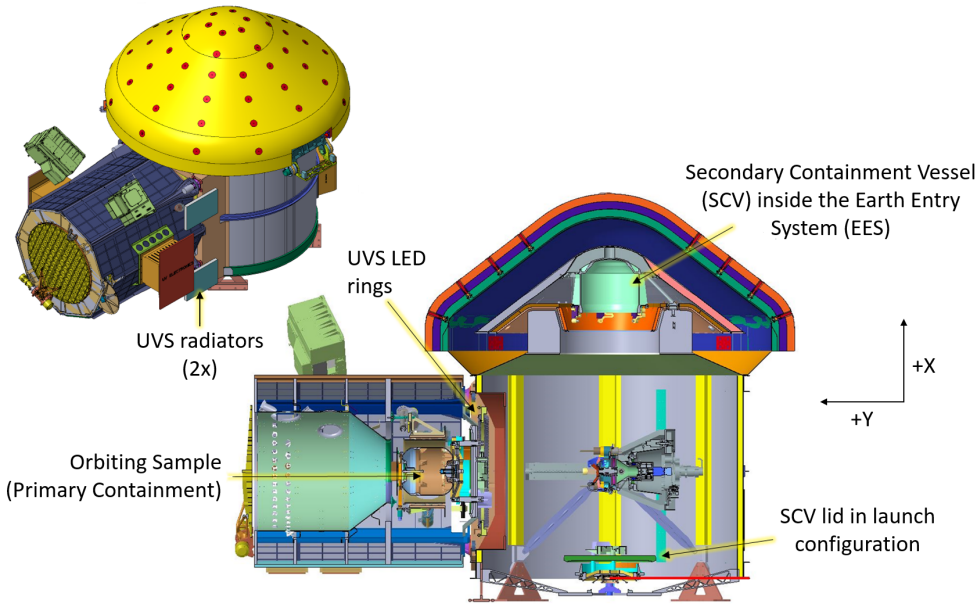

Figure 1. CCRS overview showing location of UV system (UVS). Overall dimensions of CCRS are approximately 3.4 m × 0.5 m × 2 m with total mass of about 620 kg.

While NASA's Sterilization Working Group (SWG) initially identified penetrating sterilization methods (e.g., heat or gamma radiation) [17], the MSR Program and CCRS Project identified such methods as a risk to future sample science. In contrast, a surface sterilization method such as UV imposes little to no risk to the samples protected inside the OS. The proposed UV sterilization system is expected to have lower mass than the previous heat sterilization approach [18], but as noted in the SWG report [17], UV sterilization would require additional demonstration.

In fact, like any sterilization process, the efficacy of a UV sterilization process would be subject to verification. Section 5.4.2b of NASA Technical Standard 8719.27 [19] provides for the use of industry standards in developing methods for overkill sterilization that would be used in-flight during a sample return mission. MSR has identified the overkill sterilization validation approach in ISO 11138-7 [20] as appropriate for this use. The validation must

occur under relevant environmental conditions (i.e., space vacuum, a range of temperatures and the presence of dust particles) with, in the case of UV, identical illumination parameters to those proposed for flight.

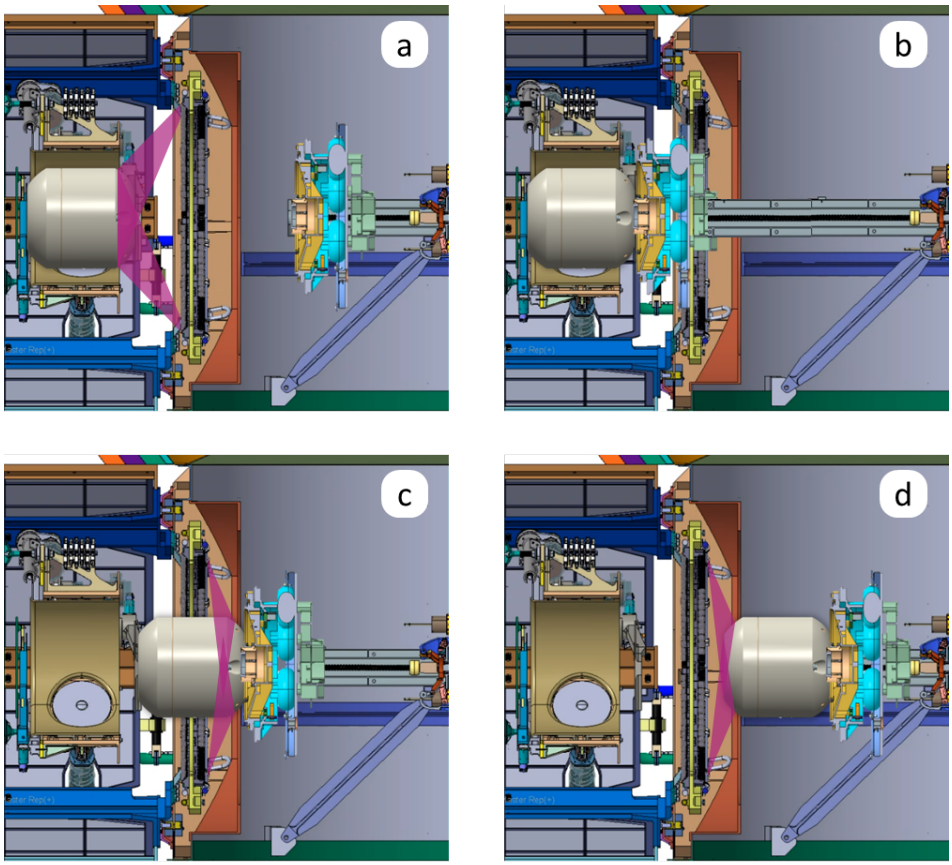

Figure 2. UV sterilization sequence. (**a**) Base of OS is irradiated. (**b**) OS is connected to Secondary Containment Vessel lids and picked up. (**c**) Sides of OS are irradiated in steps. (**d**) Lid of OS is irradiated. Note that purple shaded area is meant to show UV radiation impinging on OS. Additional details are provided in Section 4.1.

Therefore, developing a UV sterilization process necessitates the design and development of the illumination system in advance of final validation, resulting in an iterative process where performance parameters are estimated, the resulting design is tested and new performance parameters are identified until an overkill sterilization process is clearly defined.

Accommodating a spacecraft subsystem dedicated to providing a sterilizing dose of UV light would require initial estimates of the maximum mass, power and thermal allocations required. For these reasons, the MSR Program established highly conservative initial dose requirements, 2 MJ at 375 W/m^2, based on literature values for microbial reduction with UV-C light [21–23] and an understanding of the micro- and macro-scale features of the OS. This allowed system design, as discussed here, to proceed while limiting the risk that iterative testing of the system would reveal a need to increase system output and, in turn, increase impacts upon the spacecraft.

This paper presents several lessons learned while designing the UVS and is organized as follows. Section 2 describes the definition of the design requirements for the system, while Section 3 describes the selection of the light source. Section 4 provides a detailed overview of the optical design options, while Section 5 presents their reliability and redundancy approach. Section 6 describes all the optical losses that must be accounted for to meet requirements on the end-of-life irradiance. Sections 7 and 8 show the contamination control approach and approaches to thermal and power management, respectively. Section 9 briefly

describes other alternatives that were evaluated along with their features and difficulties anticipated. Finally, Section 10 provides a summary of findings and future perspectives.

2. Requirement Definition

In many applications (some examples include the sterilization of the components of a robotic sampling system that cannot be heat-treated, the sterilization of return samples collected in different containers (air, filters, rock cores, etc.), supplies sent to the International Space Station being sterilized to avoid introducing uncontrolled organisms into an experiment, etc.), a UV sterilization system would be expected to work on multiple targets, some of which might not have been fully defined when the UVS was designed. In the MSR case, project schedules resulted in the need for parallel design of the OS and UVS. However, by creating a conceptual interface surface around the OS, similar to a volume envelope, it was possible to separate the design efforts. This bounding surface is called the Outer Mold Line (OML), as shown in Figure 3.

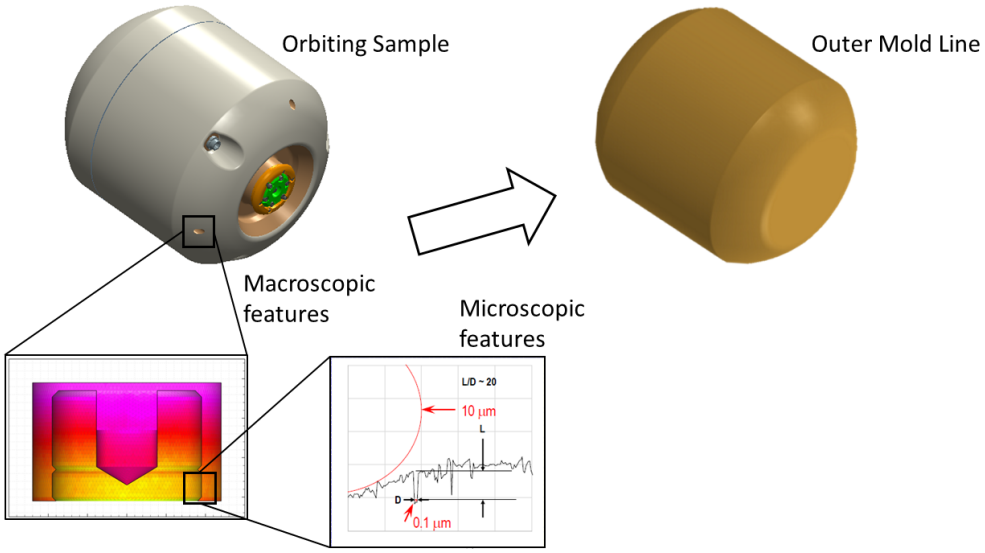

Figure 3. Defining the Outer Mold Line enables separation of requirements. UV system requirements apply only at the Outer Mold Line, while the analysis of macroscopic and microscopic shadowing drives the design of the OS, effectively separating the two development activities. The macroscopic feature highlighted in the inset on the left is a fastener, while the roughness in the inset on the right is indicated by the length, L, and depth, D, of the microscopic surface features. Particles of 0.1 and 10 µm are overlaid in red for comparison. Image courtesy of the Jet Propulsion Laboratory.

The UVS requirements are written as an irradiance (flux) and dose (fluence) delivered to the OML. A "protection factor" of 100 is specified such that the UVS irradiance delivered to the OML is 100 times higher than the estimated minimum irradiance necessary to assert the sterilization of Mars particles on the OS surface. The OS also has a "sterilizability" requirement, which constrains the macroscopic design and microscopic roughness such that the attenuation of the light from the OML to any possible Mars particle that needs to be sterilized does not violate the protection factor threshold. The protection factor must also account for shadowing by particles, whether terrestrial in origin or not. As a consequence of this division of requirements, the UVS design did not have to be concerned with how the OS geometry affected the light levels at the surface of Mars particles.

The UVS requirements also specify the peak wavelength and full width at half-maximum of the light source. This is necessary because the determination of the minimum necessary irradiance was derived as a multiple of the naturally occurring UV levels at the top of Mars' atmosphere. For a summary of the requirements, see Table 1.

Table 1. UV system illumination requirements.

Parameter	Requirement
Dose at particle	20 kJ/m^2
Peak wavelength	275–285 nm
Peak width at half-maximum	10 nm
Minimum unprotected flux [a]	3.75 W/m^2
Protective factor [b]	100

[a] Irradiance at particle surface. [b] Reduction in irradiance between Outer Mold Line and particle.

As mentioned, these requirements are generated from a conservative review of existing data [21–23] but require confirmation once the system is designed through biological testing under appropriate environmental conditions (vacuum, temperature, presence of dust particles) using flight-like illumination parameters. The MSR Program has been conducting a parallel effort to demonstrate overkill sterilization feasibility within the UVS requirements. This testing includes the identification of appropriate challenge species and estimating their survival when exposed to UV illumination at nearly identical wavelengths as the proposed UVS under ambient conditions. The UVS design team was guided to create a design with as much margin as possible to mitigate the risk of late requirement changes deriving from the biological testing results.

3. Diode Selection

Manufacturers typically produce UV diodes in batches of lots, and the light output properties of each lot vary slightly due to variations in the production processes. Vendors can screen the lots to find one that best suits a customer's needs. However, it is often not possible to achieve optimal values within all parameters. Notable parameters of interest that exhibit lot-to-lot variations include forward voltage, radiant flux, peak wavelength, spectrum half-width and thermal resistance. These parameters are specified at a reference temperature and operating current. Their variation with temperature and current may also play a role in selection. Vendors can identify and select optimal lots by weighting these variables if a relative importance is provided for each variable.

In addition, the quality of diode construction varies. A higher-performing and more expensive diode may be able to operate in an "overdriven" condition at a higher output, possibly providing more light than multiple lower-output and cheaper diodes operating at a lower current. We also found that some diodes produced significantly more light than nominally specified by the manufacturer. Diode aging rate is affected by overdriving but was not a consideration for this application. The required operational lifetime of the UVS diodes (<20 h) is quite short compared with commercial diode life expectancy (>1000 h).

4. Optical Design

4.1. CCRS Geometry

The CCRS is composed of two conjoined compartments, the Capture Enclosure (CE) and the Assembly Enclosure (AE), Figure 1. The UVS sterilization ring is located between the two compartments. The CE contains the capture cone, a large funnel with a quick-closing door; in Mars orbit, the OS enters the capture cone, the door closes, and the OS bounces around the capture cone until it has dissipated its kinetic energy. A pusher flat translates the OS down the funnel into the Orientation Mechanism (OM). At this stage, the OS is in a horizontal orientation (i.e., endcaps aligned along the y axis of the CCRS), but the base/lid orientation is unknown. In order to ensure the OS base is pointed towards the AE, the vision system cameras image the $+y$ endcap and engineers on the ground verify the OS orientation. If the orientation is wrong, the OM flips the OS by 180°. At this point, the OS is in position to be moved into the AE.

The AE contains the Robotic Transfer Assembly System (RTAS), a rotating retractable arm that grabs the OS from the CE, pulls it into the AE, rotates it up and pushes it into its final position within the EES. The end of the arm has the end effector gripper, which can

only latch with the Secondary Containment Vessel (SCV) lid. That lid has an interface that can latch to the OS base endcap but not the lid endcap. The RTAS with the end effector and SCV lid extends out through the UV ring to grab the OS from the OM. The RTAS then retracts, pulling the OS through the UVS ring and into the AE, at which point the OS is fully sterilized. Retraction can occur in any number of discrete steps as needed.

The UVS ring must be large enough to permit the SCV lid to pass through with clearance. This limits how close the source diodes can be to the OS and determines the diameter of the ring. Because these diodes emit light over a wide cone, optical concentration is required to achieve the desired irradiance at the OS OML. No perfect optical design is possible because the diodes are area rather than point sources. However, since this is not an imaging application, both compound parabolic concentrators (CPCs) and aspheric lenses are good options for narrowing the cone of light. For short working distances with wide cone angles, or for vacuum UV wavelengths, CPCs may be preferable due to the availability of high-reflectance coatings. As the working distance increases, the cone angle to maintain the irradiance decreases and the CPC length must be increased, which can quickly increase the mass and volume of the design, as well as make it more difficult to apply coatings to the interior. Fused silica is adequately transparent in UV-C wavelengths and may be formed into aspheric lenses. The UVS team modeled both options and selected aspheric microlens arrays. The final design provides the required irradiance over the full OS OML surface, including loss terms (see Section 6) and holding an additional 15% margin (see Sections 2 and 6).

4.2. Diode Performance

The UV system is nominally required to irradiate at a peak wavelength of 275–285 nm. Samples of a flight candidate light-emitting diode (LED) batch (Nichia NCSU434C) were measured at NASA's Goddard Space Flight Center to verify performance. Spectral measurements show a skewed peak distribution, which is expected for LED emission, but the non-symmetry should be taken into consideration when writing peak-width sterilization requirements. Only 67% of the energy fell within the 10 nm requirement band, and this band was near, but not exactly at, the peak of the spectrum (Figure 4). The calibrated output irradiance of the bare candidate LED and an LED + asphere system was measured and compared against model output using a vendor-supplied LED source file. The measured irradiance was systematically higher than modeled expectations, suggesting the vendor-supplied data represent the worst case and the modeled expectations are quite conservative. While a larger number of LEDs should be measured to increase statistics, the final flight LEDs chosen would be handpicked for the highest output.

Several environmental tests were conducted to confirm the flight validity of the Nichia NCSU434C 280-nm LED part type, as well as to confirm minimal optical power degradation through environmental conditions the LED is expected to experience during flight. The tests included cold storage testing, passive thermal cycling, proton radiation and burn-in testing.

Cold storage testing was conducted at −40 °C for 100 h. Before and after the 100 h cold storage, the LEDs were current-driven from 0 to 0.6 A at 25 °C, while collecting voltage, current and optical power measurements. These metrics were used to trend effects due to the cold storage. No optical power or voltage changes were observed. The tests consisted of passively cycling the thermal environment of the LEDs from −40 °C to +85 °C for a total of 500 cycles. Every 25 cycles, active voltage, optical power and spectral measurements were collected at 25 °C for data trending. The LEDs saw 0.4% optical power degradation every 25 cycles, which is acceptable within the system allocations.

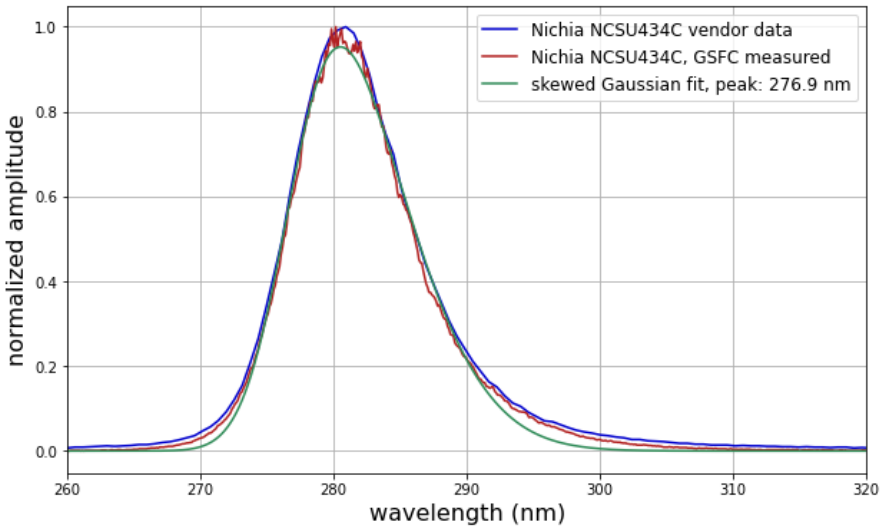

Figure 4. Nichia NCSU434C diode spectrum.

Proton radiation testing saw Nichia SU LEDs irradiated with progressively increasing proton radiation dosages. At each step, data trends were collected for active voltage, optical power and spectral measurements at 25 °C. The LEDs experienced 450 krad maximum dosage during the testing, and no gross optical power degradation was witnessed throughout.

For burn-in testing, six total LEDs saw 100 h of on time at their maximum currents per the manufacturer's recommendation (0.5 A for continuous-wave operation, 0.6 A for pulsed). Three of the LEDs were driven with continuous-wave currents, and the remaining three LEDs were driven with pulsed currents. The pulsed LEDs were tested for 1000 h at a 10 ms pulse width and 10% duty cycle to achieve 100 h of on time for comparison to the continuous-wave LEDs. Each set of LEDs was burned in at 35 °C. Throughout the burn-ins, voltage and optical power measurements were collected, ultimately showing that after 100 active hours at 35 °C the LEDs witnessed a 1–3% degradation in optical power. This is true for both continuous- and pulsed-current LEDs.

A Construction Analysis was also conducted on the Nichia NCSU434C part type, which consisted of several tests to determine whether the part was safe for flight from a construction standpoint. These tests were all held to proper Military Standards, and they consisted of an in-depth visual inspection, prohibited materials analysis, radiographic examination, internal examination through cross sectioning of the part and hermeticity testing. The Nichia SU passed each test, confirming that the construction of the LEDs is valid for spaceflight.

4.3. UVS Optomechanical Design

The bare candidate LED emits light in a relatively wide angle ($>\pm 45°$), as can be seen in Figure 5a. The UV LEDs must irradiate the OS at a distance due to mechanical constraints on the ring diameter, so the light must be concentrated to avoid loss. Single-LED + optics designs were explored, including CPCs and stand-alone aspheric lenses. However, designs with a single row of LEDs per ring, with or without optics, did not meet the OML dose requirements. Additional rows of diodes would not fit within the mechanical constraints of the system. To achieve more diodes within the space and mass limits, diodes were grouped in sets of four to form one effective LED with a distributed source footprint. The CPCs and aspheres then had to be made larger to meet the increased source size. Dosage requirements were met, but the designs did not fit within mechanical constraints. At this point, more conventional optical solutions were exhausted and the design moved to incorporate microlenses to concentrate the output of each LED while still packing LEDs relatively close together in the rings (Figure 5b).

The design solution consists of two rings of LED arrays plus microlens array optics, with a modular structure. The base ring faces $+y$, directing light towards the OS base at four distinct angles when the OS is still in the OM. The lid ring faces $-y$, directing light towards the OS sides and lid at one set angle as it is translated in free space through the ring by the RTAS (Figure 2). Each ring is composed of repeating module elements, allowing for streamlined manufacturing and integration.

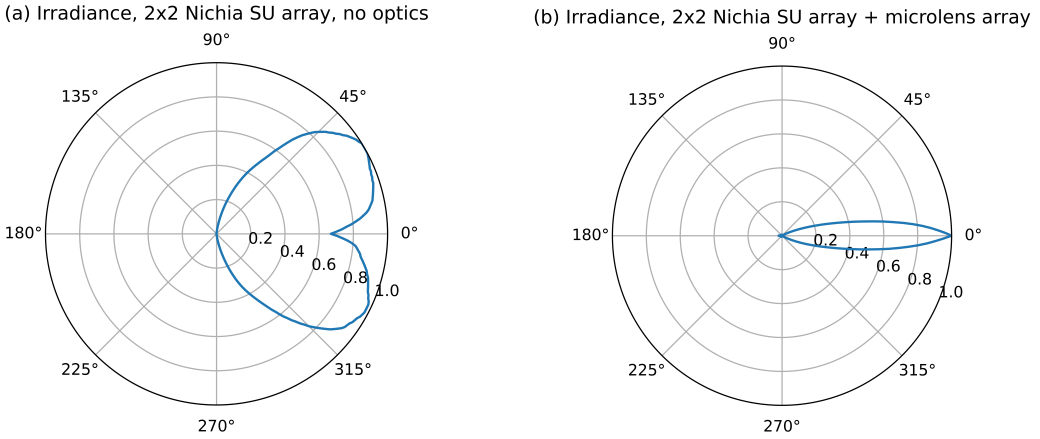

Figure 5. Dispersion of diode output. (**a**) Dispersion of bare 2 × 2 diode array. (**b**) Dispersion with aspheric microlens array.

Starting from the LED level, four diodes are mounted inside an aluminum nitride (AlN) sub-mount cavity with a bonded 2 × 2 asphere microlens array, forming a single light engine (Figure 6a). The aspheres in the microlens array design effectively concentrate each LED's radiant irradiance to a significantly narrower cone (Figure 5b), without the need for an oversized optic. Four light engines are mounted on two different module mounts to form both a base module (Figure 6b) and a lid module. Twenty-six of either base or lid modules complete a ring (Figure 7a,b).

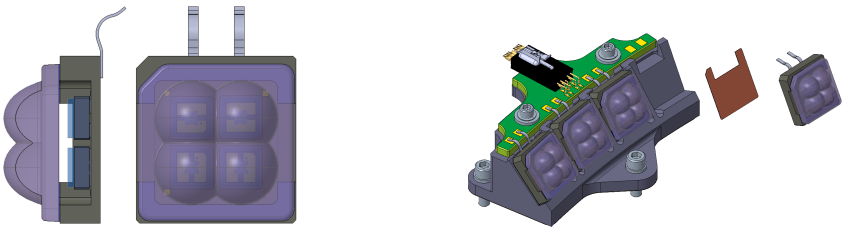

(**a**) (**b**)

Figure 6. The fundamental, modular components comprising the UV rings. (**a**) A light engine consisting of a 2 × 2 diode array and an aspheric microlens array. (**b**) A module consisting of 4 light engines, a PWB and a heat sink.

Each ring contains 104 light engines, the maximum number that can fit around the UV not-to-exceed inner diameter. Each ring module has its own Printed Wiring Board (PWB) with an 8-pin connector. The connector allows for the interdigitated wiring of the light engines so that, if a failure were to occur, the loss of irradiance could be spread around each ring (see Section 5 for additional details). The module mounts on which the light engines are mounted also serve as a heat sink to the UV optical bench, which also holds the thermal mitigation and electrical harnessing (see Section 8). The bench is connected to the Capture Enclosure (CE) via flexures. UV illumination occurs shortly after OS capture and orientation but before the CCRS' transit back to Earth. The UVS is jettisoned with the CE prior to return. The available CCRS launch mass limits the available volume within which

the UVS is required to fit. These mass and volume constraints are a significant factor in the UVS design. The total UVIA mass and mass breakdown can be found in Table 2.

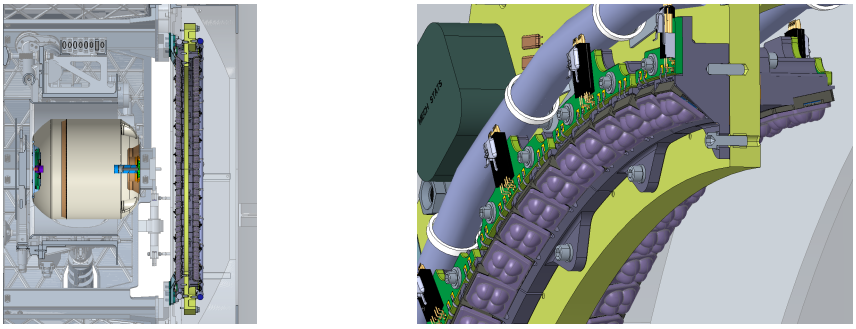

(**a**) (**b**)

Figure 7. Two UV rings mounted onto UVS optical bench. (**a**) Side view showing OS ready for irradiation. (**b**) Close-up showing modules along ring.

Table 2. UVIA mass overview.

Component	# Flight Units	Mass/Unit (kg)	Mass (kg)
UV illumination assembly			**15.9**
UVIA Module #1 assembly (base ring)	26	0.063	1.8 [a]
Module #1 assembly harnessing	1	1.1	1.2 [a]
UVIA Module #2 assembly (lid ring)	26	0.061	1.7 [a]
Module #2 assembly harnessing	1	1.1	1.2 [a]
Optical bench	1	6.99	7.7 [a]
Optical bench flexures to CE	4	0.25	1.1 [a]
UV optical bench thermal harness	2	0.5	1.2 [b]

[a] A 10% mass growth allowance is included. [b] A 15% mass growth allowance is included.

Materials selection is an important design factor due to the high levels of UV irradiance produced by the light engines. Natural and synthetic polymers, including rubbers, can lose strength and compromise surfaces by creating cracks, while silicons, metals and glasses are generally UV-stable. Coatings must not degrade under UV exposure. Within the light engine, the silicon epoxy attaching the microlens array to the sub-mount has bond line edges and bond surface areas exposed to the highest amount of UV illumination via direct illumination and stray light from scattering through the lens. Specialized testing is needed to demonstrate the silicone epoxy's UV resilience.

4.4. System Level OML Irradiance

Irradiance was modeled in ANSYS Zemax Optics Studio [24] Non-Sequential mode, with further analysis in python 3.9.7 [25]. Irradiance requirement levels were analyzed over the OS OML and included loss terms and an additional 15% margin (see Sections 2 and 6).

To avoid the contamination of the end of the robotic arm when it latches onto the OS (see Section 4.1), the portion of the OS base endcap that comes into contact with the arm must be sterilized prior to the arm's approach (Figure 2a). While in the OM, the UV base ring must irradiate the majority of the OS base endcap under static conditions. Four light-engine pointing angles are needed to irradiate the relatively large surface area. The center of the OS base is the most difficult to irradiate as it is radially farther from the UV ring and rays hit with higher angles of incidence (AOIs) closer to the apex.

The required irradiance is only met if half of the light engines point more towards the center and their overlapping footprints can compensate for the high-AOI cosine drop-off. The outer edges of the endcap are closer to the UV ring light engines and are at lower angles of incidence. However, they present a larger area, so the footprints of individual light engines overlap less and irradiance drops as the endcap curves back towards the OS sides. Complete base endcap coverage requires additional light engines, which requires

a larger ring, pushing the irradiance distance farther and increasing mass. Since the OS pickup interface does not cover the entire OS base, the current UVS ring design irradiates ~80% of the OS base (an area larger than that which is covered by the arm mechanism), and the remaining outer portion of the base endcap is irradiated by the lid ring after pickup.

After base ring operations, the robotic arm extends through the UVS ring and latches to the sterilized OS base. The OS is translated along the CCRS y axis 190 mm to the first location for lid ring operation. The lid ring irradiates the remaining outer ring of the base endcap (Figure 2c), and then the OS is translated through the ring in 25 mm discrete steps to sterilize the OS sides and lid (Figures 2c,d and 8). The axial distance of the OS is limited by a hard stop location (at which the robotic arm cannot retract any further) after it has traveled through the UV ring. This requires lid endcap irradiance to be completed with steep pointing angles at a relatively close range (Figure 2d). This physical restraint, balanced with the need to irradiate the OS base during the first lid ring step, sets the pointing angle of the lid ring light engines; all light engines in the lid ring have the same pointing angle.

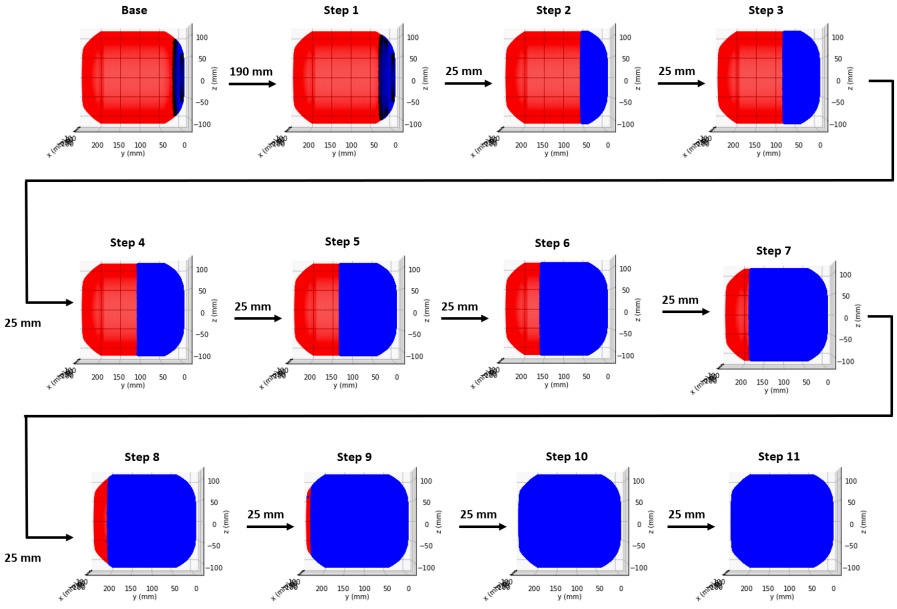

Figure 8. Irradiance coverage as the OS is stepped through the UVS. The final step is irradiating an OS end face that is not visible in this view. Blue indicates the irradiated area of the OS (red).

Preliminary Monte Carlo analysis of the full system finds that irradiance requirements are met within 99% when all error budget terms are accounted for, indicating that the design margin is robust to optical and optomechanical manufacturing, alignment/assembly and OS location uncertainty.

5. Reliability and Redundancy

Diodes for large area irradiance are typically operated as "strings" of several diodes. The UVS uses 26 parallel strings of 16 diodes in series. Optimizing the number of diodes per string was an interesting problem. Too few diodes per string required ballast, which generated extra heat with no UV benefit. Too many diodes per string put a larger fraction of the system at risk if a string failed. For purposes of assembly and testing, it was desired to have identical string lengths, which means the number of diodes must be divisible evenly by the number of strings. Each design iteration required a cycle of optical, electrical and thermal analyses.

Although LEDs are high-reliability items that tend not to "fail" in the ordinary sense as long as their operating conditions are properly controlled, each string also had current and voltage sensing and trim electronics. The optical design was evaluated to determine

if diode-level redundancy was required or if sufficient overlap between strings existed to maintain the minimum irradiance with one failed string.

For ease of manufacturing, as already discussed, diodes are grouped into light engines (four diodes) and modules (four light engines). The simplest wiring results from having one string occupy all four light engines on a module. This design produces a concentrated light deficit when a string is lost. By distributing the four light engines in a string over neighboring modules, the lost light can be spread out between operating light engines. A working design consists of strings that wire every fifth light engine such that any failed light engine would be surrounded by four operating light engines on each side (Figure 9). This layout prevents any portion of the OS from being exposed to under 375 W/m^2 due to a single string failure. However, it requires wiring some non-adjacent modules together, adding additional wiring mass and complexity.

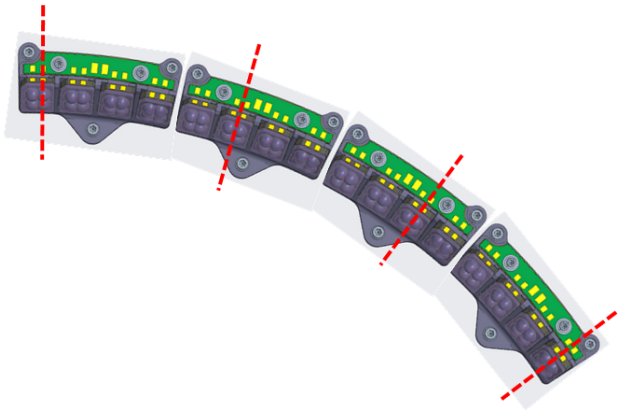

Figure 9. Every fifth light engine is wired such that any failed light engine would be surrounded by four operating on each side. This configuration meets the requirements with margin.

6. Optical Losses

To meet the requirements on the end-of-life irradiance, sources of optical loss must be accounted for. To generalize, sources of optical loss reduce the final irradiance in one of two modes: the deviation of the relative pointing angle between the UVIA and the OS or radiance degradation over operation time.

Sources of optical loss are grouped in terms of manufacturing errors, assembly errors, test knowledge uncertainty, on-orbit positional error and in-operation radiance degradation. Loss terms from manufacturing errors are controlled in the manufacturing of components. Loss terms from alignment errors can be corrected within measurement error during assembly, integration and testing. Test knowledge uncertainty is inherent to the tools used for measurement. In-orbit positional error and in-operation radiance degradation are sorted into terms of random error or systematic error and then given an allocation for the expected optical loss. After accounting for the projected optical loss atop the irradiance requirements, the current UVS design carries an additional 10% margin on end-of-life irradiance. The following subsections expand upon each of these terms, while Table 3 presents a summary.

Table 3. Optical loss allocation [a].

Pre-Launch	
Manufacturing	8.6%
Alignment	14.4%
Test	4.1%
Post-Launch	
Random loss	8.9%
Systematic loss	15.0%

[a] Predicted by analysis.

6.1. Manufacturing

Manufacturing loss allocations encompass the effects from dimensional tolerances. After establishing manufacturing tolerances with vendors and simulating the associated irradiance impact, allocations are given to the expected optical loss originating from individual manufacturing errors. These manufacturing errors include the LED chip (die) placement within the LED package, the LED package itself, the light engine (Figure 10), the lens array, the modules and the ring to which the modules are mounted (the optical bench). The stack-up of all manufacturing errors reduces the final irradiance by deviating the relative pointing between the OS and the optical components, which are the LEDs and the lens array.

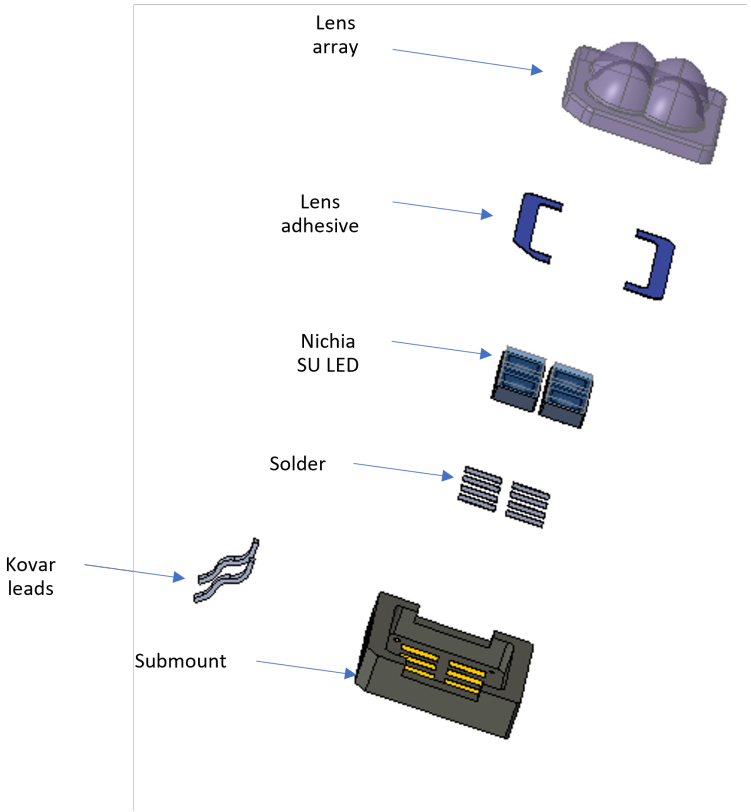

Figure 10. An exploded view of a light engine.

The largest contributors to manufacturing error are as follows: the co-planarity of the sub-mount interface to the LEDs (tolerance 25 mrad, loss 4.0%), the pattern centration of lenslets in the lens array (tolerance 0.050 mm, loss 3.4%) and the pitch pointing angle error of the module mount surface to a single light engine (tolerance 13.4 mrad, loss 3.3%). To conservatively bound the expected irradiance impact from the stack-up of manufacturing errors, irradiance losses from individual sources are aggregated by a root-sum-square. The resulting irradiance impact allocation for optical losses due to manufacturing error is 8.6%.

6.2. Alignment

Because of the constraints of the mass production of more than a thousand units, alignment errors at the light engine assembly level were considered non-correctable. The planned quantity of light engine components manufactured and aligned exceeded the necessary amount for a flight unit. After the characterization of the light engines, the best performing units were selected for flight use. At higher levels, the ability to measure and correct alignment during assembly was included in the assessment. The alignment loss terms include the LED package to the light engine, the lens array to the light engine, light engines to modules, modules to the ring and the ring to the CCRS structure.

The largest loss terms are the lens array alignment to the sub-mount (tolerance 0.200 mm, loss 13.5%) and pitch pointing angle error of the alignment between a module mount interface to a single light-engine (tolerance 9.5 mrad, loss 3.7%). The high sensitivity to these parameters is due to the steep illumination angle at the centerline of the OS endcaps (Figure 2a,d). The stack-up of all alignment errors reduces the final irradiance by deviating the relative pointing between the OS and the optical components. Irradiance losses from individual sources of alignment errors are aggregated by a root-sum-square. The resulting irradiance impact allocation for optical losses due to alignment error is 14.4%.

6.3. Test Knowledge Uncertainty

The characterization and measurement of the performance from the UVS have fundamental limits. The sources of test uncertainty include detector calibration, source non-uniformity, relative incidence angle between the detector and source (exacerbated by overlapping light sources), measurement noise and alignment errors of the test equipment. Worst-case allocations to each of the error terms were established by simulating a light engine illuminating a flat plane. The expected uncertainty for error terms can be improved with better-controlled test equipment. In developing ground support equipment, such as a baffle-mounted detector on a gimbal stage, improvements are expected for measurement noise and angular effects.

6.4. Post-Launch Random Loss

Post-launch sources of error contribute to uncertainty in the irradiance in one of two modes—the deviation of the relative pointing angle between the UVIA and the OS or radiance uncertainty. These random losses can be combined by the root-sum-square rule. The resulting allocation for this category is 8.9%.

The relative pointing angles between the OS and the optical components are expected to change non-deterministically between pre-launch integration and post-launch operation. To account for the irradiance loss due to this deviation of pointing angles, an expected percent loss allocation is given to the OS position uncertainty, thermal impact on pointing angle and vibration. The irradiance impact of the OS position uncertainty is simulated from the positioning uncertainty of the OM (for base ring illumination) and of the RTAS (for lid ring illumination). The thermal impact of temperature gradients is simulated with structural, thermal and optical performance (STOP) analysis. A vibration mode analysis provides a displacement case to evaluate the associated irradiance impact during orbit maneuvers.

Random post-launch radiance uncertainty is expected from thermal effects on LEDs and the dynamics of the electrical bus. The optical efficiency and peak wavelength of LEDs change with temperature. The electrical bus has an uncertainty on its driving current, which cascades into an uncertainty in the conversion to optical radiance.

6.5. Systematic Loss

Systematic losses include contamination (discussed in more detail in Section 7), radiation damage, diode burn-in and diode aging. Systematic losses were categorized under post-launch because most of the loss occurs in orbit. However, the burn-in occurs during ground testing. These losses are projected to predictably degrade optical performance over time, and so these losses are accounted for by an allocation corresponding to end-of-life. Rather than applying the root-sum-square rules, these predictable losses are summed, which results in a percent loss allocation of 15%.

7. Contamination Control

High-irradiance UV light can excite and break chemical bonds. In fact, this is why it is useful for sterilization. In the context of the contamination of the UVS optics, however, this is an undesirable effect because it causes the accumulation of a photo-polymerized layer of contamination. This effect is not often observed in industrial settings, because oxygen can

react with the excited bonds and remove contamination from surfaces. During laboratory burn-in testing of diodes, no contamination build-up was observed.

The presence of chemicals subject to photo-polymerization must be controlled in vacuum testing and on-orbit. This means heating organic materials under a vacuum (bakeout) to remove chemical species that can diffuse to the surface and become volatile. That diffusion and desorption process is known as outgassing. Starting from a throughput loss allocation, a requirement for the outgassing rate was derived.

Using a conservative absorption coefficient, throughput loss was converted to a thickness of deposition. Although the optical properties of the deposited material vary depending on the chemicals and degree of cross-linking, the variation at 280 nm is not large [26]. At high UV intensities, it is safe to assume that the polymerization process is limited by the arrival rate of molecules. The allowable thickness divided by the time during which the system is operating provides a mass flux limit at the UVS. The time must include both flight and ground testing. This mass flux is then allocated to sources throughout the CCRS system. Items which are warm have higher outgassing rates (both diffusion and desorption are strongly temperature-dependent), so these items should receive a larger allocation. Further refinement is possible by modeling the transport of molecules through the structure and accounting for the escape of some of the contaminants to space.

One final consideration must be applied, and that is the polymerization of contaminants on the OS while it is irradiated. To prevent the OS design team from having to know the CCRS outgassing rate when performing their protection factor calculations, the loss due to the contamination of the OS is included in the UVS optical degradation budget. This essentially cuts the allowable deposition in half when performing the calculations.

During the cruise phase from Earth to Mars, some contamination may accumulate on the UVS optics simply because they are relatively cold compared to some outgassing sources. To prevent the polymerization of these contaminants, the UVS has an operational heater that is turned on before the diodes. The contaminants quickly desorb from the optics once they reach room temperature.

Contamination by loose particles also reduces the output of the UVS. Typical cleaning and integration in cleanrooms keep the particle contamination low enough that the expected area coverage is <0.1%. To allow a margin for Mars particles redistributed during capture and orientation of the OS, an area coverage of 0.25% is used. These values are low enough that particles are assumed to be completely opaque, regardless of size or composition.

On the OS, where a particle may land in a position that shadows something needing sterilization, the size distribution and UV transmission of the particles become important. The quantity, type and size distribution of expected particles were provided to MSR for inclusion in their protection factor analyses.

8. Thermal and Power Management

UV diodes have a low efficiency for converting power into light. Operating a high-flux UV system generates a large amount of heat that must be removed. To reduce the size of the radiators, the diodes are operated in a pulsed mode with a duty cycle of a few percent. This results in an average power dissipation of 25 W for a peak power of 1900 W, where the average power is limited by the capability of the radiators and heat pipes. Thermal analysis is accomplished at a preliminary design level, showing that the peak and average power levels are acceptable with a 30% available margin at launch. The peak current and power supplied to the LED strings are determined by LED life testing and power available from the ERO spacecraft when solar arrays are illuminated. UV illumination would be applied over long periods (hours-days) under the premise that any putative organisms present would be dormant due to the space vacuum and, potentially, low temperature. This allows operating in a pulsed mode.

If the peak current needs to be limited (for example, because of battery limitations during eclipse), it is possible to operate sections of the ring in sequence. The low duty cycle means that all sectors could be irradiated within each interval between pulses, so the

operating time is not extended. However, it is necessary to overlap the sector exposures so that some areas of the target receive extra dose. This is inefficient but not a violation of requirements. Also, the layout of diode strings would have to accommodate this division.

9. Alternate Architectures

When evaluating the use of UV diodes for the sterilizing mode, several other possibilities were examined. While a discussion of the sterilization effectiveness of these options is outside the scope of this paper, which is focused on hardware design and implementation, the design features and difficulties anticipated are discussed here to aid future projects.

9.1. UV Chamber

A dedicated chamber with a reflective interior that is filled with UV was an attractive concept because the entire OS could be exposed at one time. Difficulties included the number of diodes and total power required and the means of holding and passing the OS through such a chamber without shadowing parts of the OS.

9.2. Mobile UV Source

Rather than moving the OS through the UVS, we considered holding the OS stationary and moving a UV source around it. This results in a smaller UV source drawing less power and perhaps allows the UV source to become closer to the OML. However, removing heat from a mobile source requires conduction through a flexible path, which is more difficult than the heat pipes used by the current design. In addition, the smaller the irradiated area, the longer it takes to apply the required dose to the entire surface. Additionally, moving and flexing components are potential sources of fatigue and other mechanical failures.

9.3. Concentrated Natural UV

Mirrors or windows could be used to bring solar UV to the OS. Because of the protection factor, a concentration above the natural irradiance is required.

9.4. Mercury Vapor Lamps

Either low- or medium-pressure lamps can produce UV with higher efficiency than diodes. A quick look suggested that quartz tube lamps can be made flight-compatible, but the technology development effort for UV diodes was better understood when we made the selection.

9.5. UV Laser Diodes

Laser diodes can provide a very high irradiance, but in a very small space. Nonetheless, they require technology maturation.

9.6. Chemical Sterilization

Ethylene oxide, hydrazine and vapor hydrogen peroxide efficiently sterilize surfaces. However, these chemicals have the potential to create a science contamination risk. Hydrazine has health hazards which make ground testing of the system more complicated, and controlling the gas has its own complications. The OS must be placed in a sealed chamber, which is filled to some pressure, and then the gas must be vented with spacecraft compensation for the thrust effect. Ethylene oxide also requires humidity preconditioning and extended time holding pressure in the chamber.

9.7. Plasma/Ion Sterilization

Plasma/ion sterilization was looked at during the re-architecture of the sterilization system, and the following main drawbacks were identified: electromagnetic interference problems (the most concerning one), the ability to hold pressure and the fact that it suffers from shadowing by particles.

9.8. Radiation

A penetrating source like Cobalt-60 eliminates much of the concern over the protection factor. However, the handling of radioactive sources presents both ground hazards and launch restrictions. In addition, it poses problems to sample integrity, diminishing the return to science.

9.9. Active Surfaces

Some surface coatings interact with microbial life, with or without photo-activation. However, the requirement for an optical system to locate the OS in orbit severely limited the acceptable finish options for the OS.

10. Discussion

The authors hope that the lessons learned during the formulation phase of the CCRS UV system may prove useful to future projects.

During the development of the requirements, the definition of a radiation interface (the Outer Mold Line) between the source and the target object allowed design activities to proceed in parallel; small changes in the OS surface features could be ignored by the UVS team, allowing for rapid development and modeling. However, the features can block direct irradiance from small nooks and crannies, and multiscatter analysis and testing are needed to verify that the 100× protection factor is sufficient to account for these and reduce the risk of late-stage design changes.

The high-irradiance requirement combined with mass and thermal limitations greatly constrains the system design. UV LEDs without concentration (an oven baking approach) require a significantly higher number of LEDs. More traditional concentrators such as CPCs and single aspheres are bulkier and grow inefficient as the light source moves off axis, so increasing the number of LEDs under a single optic requires growing the optics, while increasing the number of LED + optic units adds substantial mass. The chosen design of fused silica microlens arrays with relatively steep curvatures is still being constructed and tested, so manufacturability will need to be confirmed.

UV diodes vary in their quality of construction and performance. Obtaining test articles may reveal candidates that perform better than the vendor specifications, easing the need to carry as great a margin elsewhere. Operating in a pulsed mode creates opportunities for thermal and power management by carefully sequencing the diodes.

Finally, contamination control, especially with respect to outgassing sources, is important for vacuum UV systems.

This document is being made available for information purposes only. The decision to implement Mars Sample Return will not be finalized until NASA's completion of the National Environmental Policy Act (NEPA) process. In addition, as part of the NASA response to the recent MSR Independent Review Board's report [27] and in light of the current budget environment, the MSR Program is undergoing a consideration of changes in its mission architecture. This work is based upon the previous baseline MSR architecture in which ERO-CCRS would return the OS to Earth within approximately five years of landing on Mars to retrieve samples collected by the Perseverance rover. The CCRS Project completed system development to a Preliminary Design Review level of maturity in mid-December 2023, after which it was stopped indefinitely pending the results of the re-architecture effort.

Author Contributions: Conceptualization, D.W.H., G.C., F.A.P., T.C.H. and F.M.; Formal analysis, T.C.H., L.L.S., L.S., O.T., H.Y., T.J.E., S.I., N.M.N., B.J.B., D.W.H., R.G.S., A.K., G.B.S., K.A.S., L.O., D.E.J. and W.J.T.; Funding acquisition, F.A.P.; Investigation, D.E.J., W.B.C., T.C.H. and C.D.H.; Methodology, F.M., T.C.H., T.J.E. and O.T.; Project administration, F.A.P., R.D., T.C.H. and W.M.M.; Resources, F.M. and V.J.C.; Software, T.C.H., O.T., H.Y. and B.R.B.; Supervision, F.M. and G.C.; Validation, T.C.H., D.E.J. and W.J.T.; Visualization, D.W.H., G.C., T.C.H. and T.J.E.; Writing—original draft preparation, D.W.H., G.C. and T.C.H.; Writing—review and editing, D.W.H., G.C., F.A.P., T.C.H., F.M., V.J.C., W.B.C., T.J.E., L.O., O.T., W.J.T., H.Y. and R.G.S. All authors have read and agreed to the published version of the manuscript.

Funding: Funding provided by the National Aeronautics and Space Administration and the European Space Agency is gratefully acknowledged.

Data Availability Statement: The data presented in this study are available in the article.

Acknowledgments: The authors would also like to acknowledge Brian Clement at the Jet Propulsion Laboratory for insightful technical discussions and feedback.

Conflicts of Interest: Author Brian R. Bean was employed by the company Intuitive Machines. Author Berton J. Braley was employed by the company Lentech, Inc. Author Ratna Day was employed by the company ASRC Federal. Authors Stefan Ioana and Nicholas M. Nicolaeff were employed by the company Aerodyne Industries, LLC. Author Dillon E. Johnstone was employed by the company Science Systems and Applications, Inc. Authors Lawrence Ong, Laurie L. Seide and Honam Yum were employed by the company KBR, Inc. Author Kevin A. Smith was employed by the company Design Interface, Inc. Author Oscar Ta was employed by the company Genesis Engineering Solutions, Inc. The remaining authors declare that the research was conducted in the absence of any commercial or financial relationships that could be construed as a potential conflict of interest.

Abbreviations

The following abbreviations are used in this manuscript:

AOI	angle of incidence
AE	Assembly Enclosure
CE	Capture Enclosure
COSPAR	Committee on Outer Space Research
CCRS	Capture, Containment and Return Systems
CPC	compound parabolic concentrator
EES	Earth Entry System
ERO	Earth Return Orbiter
LED	light-emitting diode
MDPI	Multidisciplinary Digital Publishing Institute
MSR	Mars Sample Return
NASA	National Aeronautics and Space Administration
NEPA	National Environmental Policy Act
OM	Orientation Mechanism
OML	Outer Mold Line
OS	Orbiting Sample
PWB	Printed Wiring Board
RTAS	Robotic Transfer Assembly System
SCV	Secondary Containment Vessel
UV	Ultraviolet
UVIA	Ultraviolet illumination assembly
UVS	Ultraviolet system

References

1. Beaty, D.; Grady, M.; McSween, H.; Sefton-Nash, E.; Carrier, B.; Altieri, F.; Amelin, Y.; Ammannito, E.; Anand, M.; Benning, L.; et al. The Potential Science and Engineering Value of Samples Delivered to Earth by Mars Sample Return. *Meteorit. Planet. Sci.* **2019**, *54*, 667–671. [CrossRef]
2. Haltigin, T.; Hauber, E.; Kminek, G.; Meyer, M.; Agee, C.; Busemann, H.; Carrier, B.; Glavin, D.; Hays, L.; Marty, B.; et al. Rationale and Proposed Design for a Mars Sample Return (MSR) Science Program. *Astrobiology* **2022**, *22*, S-27–S-56. [CrossRef] [PubMed]
3. Grady, M.; Summons, R.E.; Swindle, T.; Westall, F.; Kminek, G.; Meyer, M.; Beaty, D.; Carrier, B.; Haltigin, T.; Hays, L.; et al. The Scientific Importance of Returning Airfall Dust as a Part of Mars Sample Return (MSR). *Astrobiology* **2022**, *22*, S-176–S-185. [CrossRef] [PubMed]
4. Swindle, T.; Atreya, S.; Busemann, H.; Cartwright, J.; Mahaffy, P.; Marty, B.; Pack, A.; Schwenzer, S. Scientific Value of Including an Atmospheric Sample as Part of Mars Sample Return (MSR). *Astrobiology* **2022**, *22*, S-165–S-175. [CrossRef] [PubMed]
5. Carrier, B.; Beaty, D.; Hutzler, A.; Smith, A.; Kminek, G.; Meyer, M.; Haltigin, T.; Hays, L.; Agee, C.; Busemann, H.; et al. Science and Curation Considerations for the Design of a Mars Sample Return (MSR) Sample Receiving Facility (SRF). *Astrobiology* **2022**, *22*, S-217–S-237. [CrossRef] [PubMed]
6. NASA Office of Safety and Mission Assurance. *Planetary Protection Provisions for Robotic Extraterrestrial Missions*; NASA Procedural Requirements (NPR) 8715.24; NASA Office of Safety and Mission Assurance: Washington, DC, USA, 2021.

7. *ECSS-U-ST-20C*; Space Sustainability—Planetary Protection. European Cooperation for Space Standardization: Noordwijk, The Netherlands, 2019.
8. COSPAR Panel on Planetary Protection. COSPAR Policy on Planetary Protection. *Space Res. Today* **2021**, *211*, 12–25. [CrossRef]
9. United Nations General Assembly. *2222 (XXI). Treaty on Principles Governing the Activities of States in the Exploration and Use of Outer Space, Including the Moon and Other Celestial Bodies*; United Nations General Assembly: New York, NY, USA, 1967; Article IX.
10. Cataldo, G.; Affentranger, L.; Clement, B.G.; Glavin, D.P.; Hughes, D.W.; Hall, J.; Sarli, B.V.; Szalai, C.E. The Planetary Protection Strategy of Mars Sample Return's Earth Return Orbiter Mission. *J. Space Saf. Eng.* **2024**, *11*, 374–384. [CrossRef]
11. Farley, K.; Williford, K.; Stack, K.; Bhartia, R.; Chen, A.; de la Torre, M.; Hand, K.; Goreva, Y.; Herd, C.D.; Hueso, R.; et al. Mars 2020 Mission Overview. *Space Sci. Rev.* **2020**, *216*, 142. [CrossRef]
12. Scheller, E.; Hollis, J.; Cardarelli, E.; Steele, A.; Beegle, L.; Bhartia, R.; Conrad, P.; Uckert, K.; Sharma, S.; Ehlmann, B.; et al. Aqueous alteration processes in Jezero crater, Mars—implications for organic geochemistry. *Science* **2022**, *378*, 1105–1110. [CrossRef] [PubMed]
13. Wiens, R.; Udry, A.; Beyssac, O.; Quantin-Nataf, C.; Mangold, N.; Cousin, A.; Mandon, L.; Bosak, T.; Forni, O.; McLennan, S.; et al. Compositionally and density stratified igneous terrain in Jezero crater, Mars. *Sci. Adv.* **2022**, *8*, eabo3399. [CrossRef] [PubMed]
14. Sharma, S.; Roppel, R.; Murphy, A.; Beegle, L.; Bhartia, R.; Steele, A.; Hollis, J.; Siljeström, S.; McCubbin, F.; Asher, S.; et al. Diverse organic-mineral associations in Jezero crater, Mars. *Nature* **2023**, *619*, 724–732. [CrossRef] [PubMed]
15. Sarli, B.V.; Bowman, E.; Cataldo, G.; Feehan, T.B.; Green, T.; Gough, K.; Hagedorn, A.; Hudgins, P.; Lin, J.; Neuman, M.; et al. NASA's Capture, Containment, and Return System: Bringing Mars Samples to Earth. *Acta Astronaut.* **2024**, *online*. [CrossRef]
16. Geelen, K.; Sutherland, O.; Baglioni, P.; Spoto, F.; Huesing, J.; Haldemann, A.; Beyer, F.; Schoonejans, P.; Accomazzo, A.; Loureiro, T.; et al. Mars Sample Return Campaign—Status of the ESA provided Elements. In Proceedings of the International Astronautical Federation, 72nd International Astronautical Congress, Dubai, United Arab Emirates, 25–29 October 2021.
17. Craven, E.; Winters, M.; Smith, A.L.; Lalime, E.; Mancinelli, R.; Shirey, B.; Schubert, W.; Schuerger, A.; Burgin, M.; Seto, E.P.; et al. Biological safety in the context of backward planetary protection and Mars Sample Return: Conclusions from the Sterilization Working Group. *Int. J. Astrobiol.* **2021**, *20*, 1–28. [CrossRef]
18. Cataldo, G.; Childs, B.; Corliss, J.; Feehan, T.; Gage, P.; Lin, J.; Mukherjee, S.; Neuman, M.; Pellerano, F.; Sarli, B.; et al. Mars Sample Return—An Overview of the Capture, Containment and Return System. In Proceedings of the International Astronautical Federation, 73rd International Astronautical Congress, Paris, France, 18–22 September 2022.
19. *NASA Technical Standard 8719.27*; Implementing Planetary Protection Requirements for Space Flight. NASA Office of Safety and Mission Assurance: Washington, DC, USA, 2022.
20. *ISO 11138-7:2019*; Sterilization of Health Care Products, Biological Indicators, Part 7: Guidance for the Selection, Use and Interpretation of Results. International Organization for Standardization: Geneve, Switzerland, 2019.
21. Beck, S.E.; Rodriguez, R.A.; Linden, K.G.; Hargy, T.M.; Larason, T.C.; Wright, H.B. Wavelength dependent UV inactivation and DNA damage of adenovirus as measured by cell culture infectivity and long range quantitative PCR. *Environ. Sci. Technol.* **2014**, *48*, 591–598. [CrossRef] [PubMed]
22. Beck, S.E.; Hull, N.M.; Poepping, C.; Linden, K.G. Wavelength-dependent damage to adenoviral proteins across the germicidal UV spectrum. *Environ. Sci. Technol.* **2018**, *52*, 223–229. [CrossRef]
23. Zammuto, V.; Fuchs, F.M.; Fiebrandt, M.; Stapelmann, K.; Ulrich, N.J.; Maugeri, T.L.; Pukall, R.; Gugliandolo, C.; Moeller, R. Comparing spore resistance of Bacillus strains isolated from hydrothermal vents and spacecraft assembly facilities to environmental stressors and decontamination treatments. *Astrobiology* **2018**, *18*, 1425–1434. [CrossRef]
24. Ansys. Zemax OpticStudio. Available online: https://www.ansys.com/products/optics/ansys-zemax-opticstudio (accessed on 25 March 2024).
25. Python Software Foundation. Python. Available online: https://www.python.org (accessed on 26 March 2024).
26. Arnold, G.S.; Luey, K.T. Photochemically deposited contaminant film effects. In *Optical System Contamination V, and Stray Light and System Optimization*; Breault, R.P., Pompea, S.M., Glassford, A.P.M., Breault, R.P., Pompea, S.M., Eds.; International Society for Optics and Photonics, SPIE: Denver, CO, USA, 1996; Volume 2864, pp. 269–285.
27. Figueroa, O.; Kearns, S.; Boll, N.; Elbel, J. Mars Sample Return (MSR) Independent Review Board-2 Final Report. NASA, 1 September 2023. Available online: https://www.nasa.gov/wp-content/uploads/2023/09/mars-sample-return-independent-review-board-report.pdf (accessed on 21 May 2024).